ACS Chemical Neuroscience

pubs.acs.org/chemneuro Research Article

Specific Key-Point Mutations along the Helical Conformation of Huntingtin-Exon 1 Protein Might Have an Antagonistic Effect on the Toxic Helical Content's Formation

Sanda Nastasia Moldovean and Vasile Chiş*

Cite This: ACS Chem. Neurosci. 2020, 11, 2881−2889 Read Online

ACCESS | Metrics & More | Article Recommendations

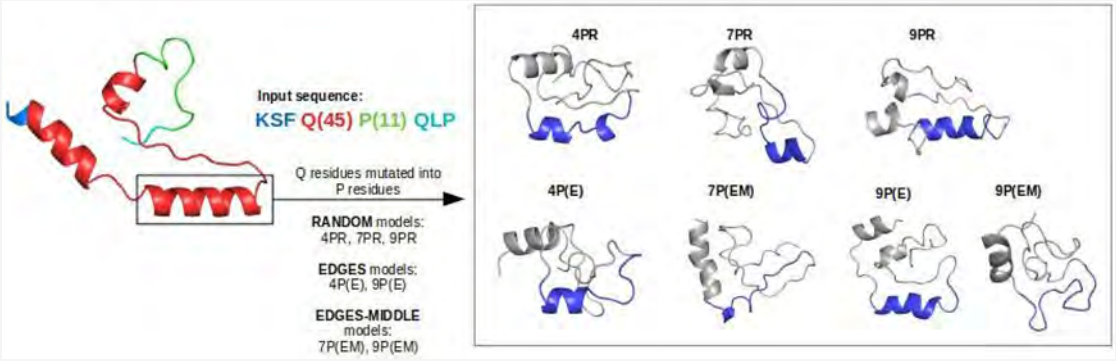

ABSTRACT: The polyglutamine tract length represents a key regulator for the Huntington's disease toxicity level and its aggregation rates, often being related to helical structural conformations. In this study, we performed all-atom MD simulations on mutant Huntingtin-Exon1 protein with additional mutation spots, aiming to observe the corresponding structural and dynamical changes at the level of the helix. The simulated structures consist of three sets of Q residue mutations into P residues (4P, 7P, and 9P), with each set including different spots of mutations: random along the mutant sequence (R models), at the edges of the helix (E models), as well as at the edges and in the middle of the helix (EM models). At the helical level, our results predict less compactness profiles for a higher number of P mutations (7P and 9P models) with particular mutation spots at the edges and at the edges-middle of the helix. Moreover, the C-alpha atom distances decreased for 7P and 9P models in comparison to 4P models, and the RMSF values show the highest fluctuation rates for 9P models with point mutations at the edges and in the middle of the helix. The secondary structure analysis suggests greater structural transitions from α-helices to bends, turns, and random coils for 7P and 9P models, particularly for point mutations considered at the edges and in the middle of the helical content. The obtained results support our hypothesis that specific key-point mutations along the helical conformation might have an antagonistic effect on the toxic helical content's formation.

KEYWORDS: *Huntington's disease, polyglutamine tract, proline-rich domain, helical conformation, neurodegeneration, molecular dynamics*

INTRODUCTION

Huntington's disease (HD) is a rare, inherited disease described by progressive loss of the nerve cells in the brain. Because of the genetic mutation that takes place at the level of the first exon (Ex.1), HD is characterized by movement disorders, physical and behavioral changes, cognitive disorders, and psychiatric conditions as well.[1]

The formation of polyglutamine (polyQ) tracts is one of the most debated issues in the literature, focusing on amyloid-like fibrils formation.[2,3] Considering that the mutation consists of additional glutamine (Q) residues, the mutated structures are able to form complementary interfaces with identical segments.[4,5] Consequently, amyloid-like fibrils are considered to be formed through assembly of steric zipper two self-complementary β-sheets.[4] On the other hand, this particular conformational assembly mechanism was found for a large variety of proteins, although not all of them presented the β-sheet configuration. A general assumption for this conformational behavior would be that β-sheet formation mainly

Received: July 30, 2020
Accepted: August 10, 2020
Published: August 10, 2020

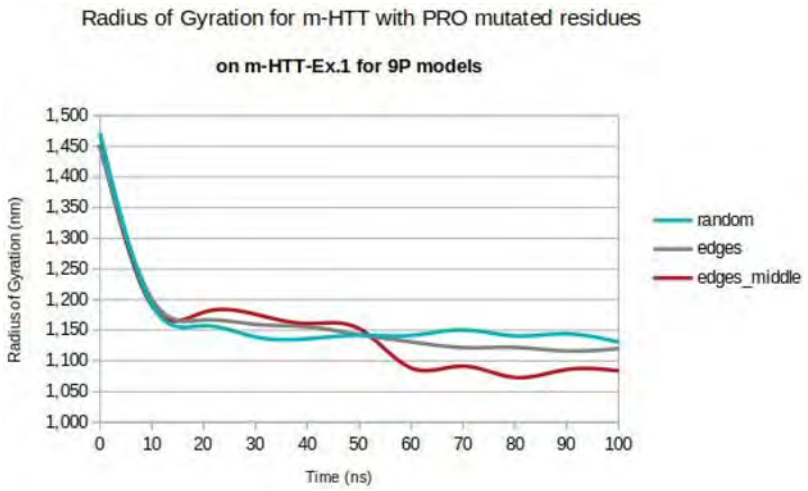

Figure 1. Radius of gyration plots for nine PRO models.

depends on specific amino acid sequences.[4,6] Starting from this hypothesis, the present study focuses on particular sequences that might have a reverse effect on the mutation, but at the helical level.

The evolution of neurotoxic conformations of mutant Huntingtin (m-Htt) protein are not stand-alone processes, and the implications of the other regions flanking the polyQ tract (N17 terminal domain, for example)[7] are being considered as a fundamental approach for a better understanding of the polyQ aggregation mechanism.

From the same perspective, proline rich domains (PRDs) have been extensively discussed in the literature,[8−10] especially because of the amino acid's distinctive structure. The cyclic side chain of the proline residue reduces its conformational flexibility, therefore affecting the secondary structure (SS) of different nearby interacting partners.[9] Another point of interest is that proline residues cannot act as hydrogen bond donors, because when the amino acid is involved in a peptide bond, the amide proton is being replaced by a CH_2 group. On the other hand, the proline residue is a strong hydrogen bond acceptor.[9] Yet another important feature is that many PR sequences can contain glutamine residues as well, as it is found in the huntingtin protein sequence. Interestingly, proline is known to disrupt α-helix and β-sheet structures, even though it is commonly found at the beginning of these particular conformations.[6,8,9] For extended PRDs, proline can also adopt loops considered to act as flexible linkers between different parts of the protein which makes the structural dynamics of this residue even more interesting if we take into account that loops are generally being exposed to solvents.[9,10]

At the level of huntingtin mutants (m-Htt), the toxicity levels were shown to increase for higher aggregation rates allowing for β-sheet structure formation.[11] The exact role of PRDs at the mutant level remains unknown. However, it is generally considered that proline tracts might be strictly involved in protein−protein interacting mechanisms, especially because, at the N-terminal domain, for wild type (WT) structures, the deletion of proline residues had no significant impact on its structural behavior.[12] Also, previous studies[13−16] have described the influence of PRD on the HTT mutant with P residues situated at the flanking region level; therefore, our interest was oriented to the impact of the P residues on the conformational changes of the polyQ tract.

RESULTS AND DISCUSSION

Radius of Gyration. *Mutant Htt Protein Compactness Level.* The compactness level of a protein represents a key structural parameter related to its folding/unfolding processes. The native states (the starting folded conformations) of the mutants were clearly altered when the Q residues were mutated into P residues. All of the structures started from R_g values around 1.45−1.47 nm. For random models, the R_g values showed variations between 7PR models and 9PR models from 1.15 to 1.18 nm. The 4P mutation models (4PR and 4P(E)) presented the same averaged R_g value of 1.15 nm. It is worth noting that for the random models the number of Q mutated residues along the helix is much lower in comparison to the other models were all the proline residues were concentrated mainly at the helical level.

In contrast, when the proline residues were situated at the edges or at the edges and in the middle of the helix, the R_g values presented a significant decrease. As a result, we observed that the structure compactness decreases with the increased number of mutated P residues. Furthermore, this decrease was seen to be related not only to the number of mutations but also to the particular spots along the helix where Qs were mutated into Ps (Figure 1).

For 7P mutation points, the R_g averaged value of 1.16 nm for random spots presented a slight increase to 1.17 nm for edges and middle spots. In contrast, from the 9P random model with R_g of 1.18 nm, the model where the proline residues were situated at the edges and in the middle of the helix presented a decreased R_g value of 1.16 nm. After 50 ns of simulation time, the largest decreases in R_g values were observed for the edges-middle models (Figure 1) with the highest compactness level for the 9P(EM) model.

Radius of Gyration on the Region of Interest. The R_g of the helical content was measured with *gmx analysis tools* by using an indexed group of atoms comprising the range between the amino acid residue 16 and 30, respectively.

At the helical level, the random models presented similar gyration behavior. The average values for 4PR and 9PR were 0.79 and 0.78 nm, while the R_g value for 7PR model was 0.77 nm. This result might imply the fact that, at this level, the relevance of P mutated residue number is reduced. On the other hand, when particular mutated spots were considered (Figure 2), the R_g values pointed out significant variations

https://dx.doi.org/10.1021/acschemneuro.0c00493
ACS Chem. Neurosci. 2020, 11, 2881−2889

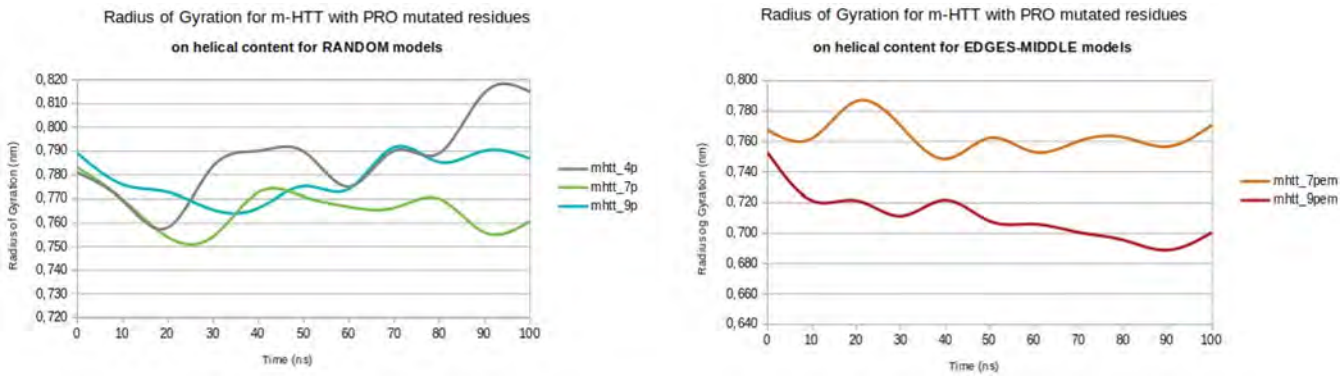

Figure 2. Radius of gyration variations for random models (left) and for edges-middle models (right) with mutation points at the level of the helix.

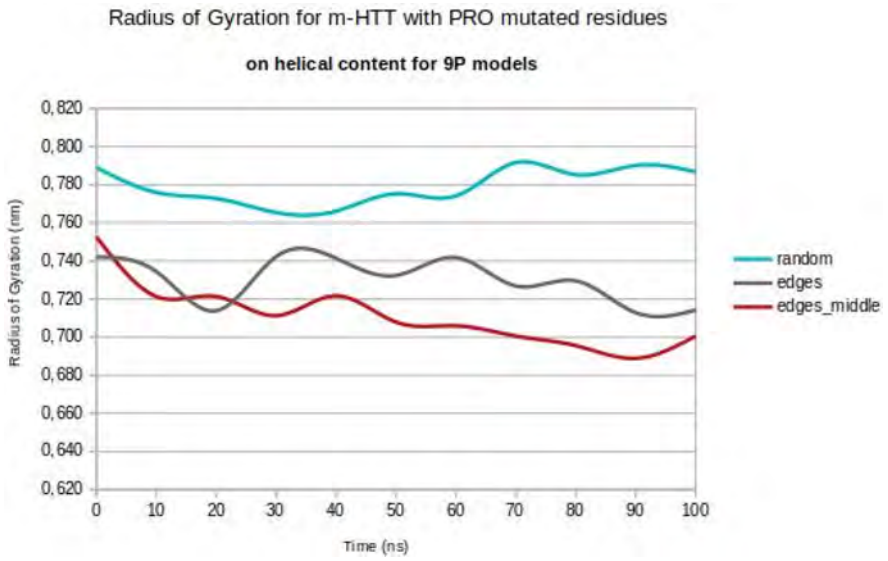

Figure 3. Radius of gyration at the helical level for nine PRO models.

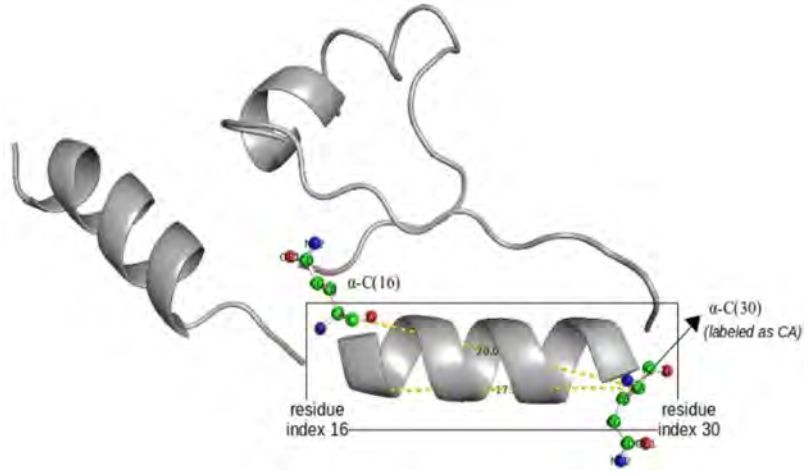

Figure 4. Schematic representation of the indexed group of atoms used for α-C(16) and α-C(30) distance measurements.

which were correlated with disruptions of the helical conformation.

At the helical level, the R_g measurements showed decreased values for higher number of P mutated residues situated at the edges of the helix (0.74 nm for 4P model and 0.73 nm for 9P model) and even lower values for structures with point mutations at the edges and in the middle of the helix (0.71 nm for 9P model with point mutations at the edges and in the middle of the helix) (Figure 3). These fluctuations were associated with large conformational changes. Moreover, the resulted unfolding states at the level of the helix were strongly related to the reduced motifs for helical secondary structure conformations.

https://dx.doi.org/10.1021/acschemneuro.0c00493
ACS Chem. Neurosci. 2020, 11, 2881−2889

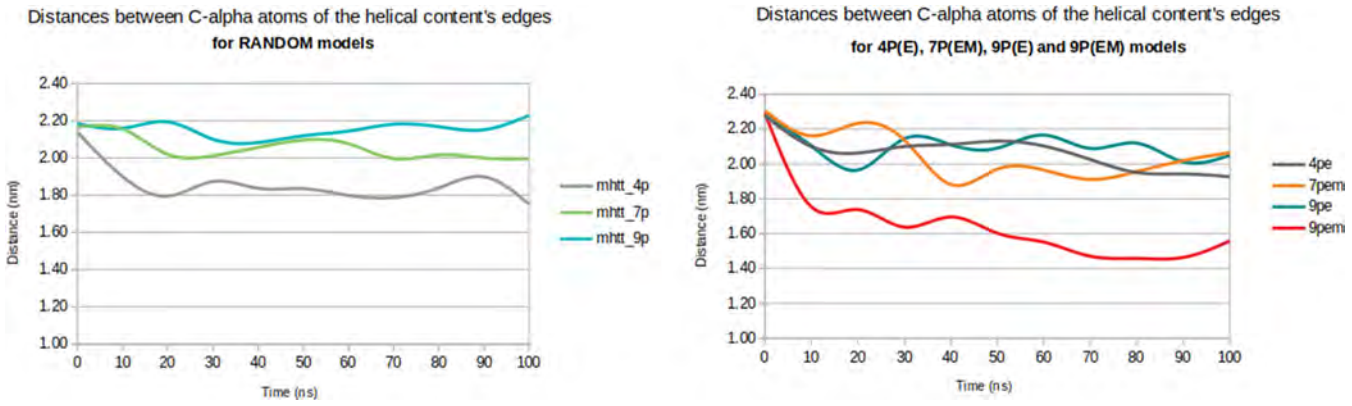

Figure 5. Plotted distances between α-C(16) and α-C(30) for random, edges, and edges-middle models.

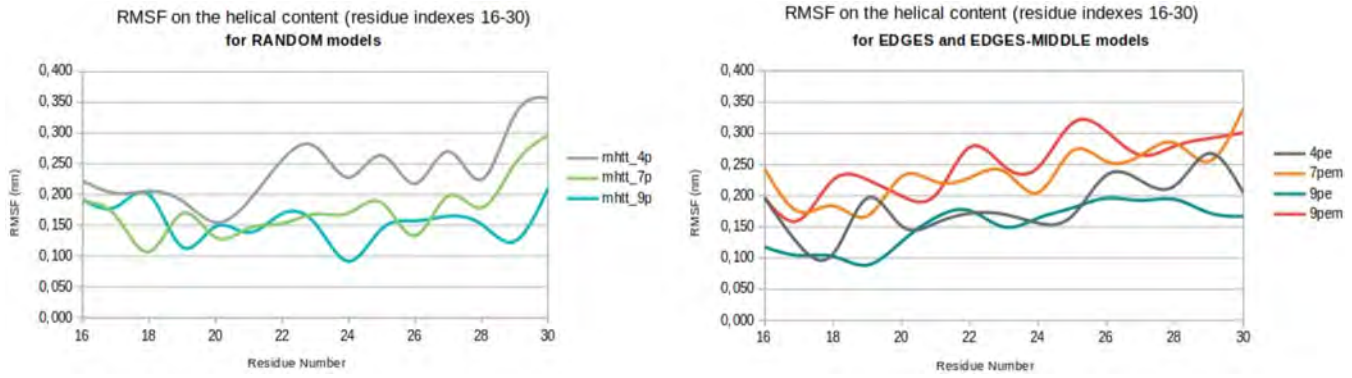

Figure 6. RMSF per residues (for residue numbers 16−30) for random models (left) and for edges and edges-middle models (right).

As shown in Figure 3, a higher number of mutations implies greater importance for the spot of mutations. The 4PR model presented the highest R_g value of 0.79 nm, while the lowest average value of 0.71 nm was obtained for 9P mutations at the edges and in the middle of the helix (9P(EM)).

Distances between C-α Atoms. Distances between the geometrical centers of α-carbon atoms were also measured in order to establish a correlation between R_g values and the helical disruptions. The edges of the helix were considered as a single indexed group of atoms. From all the constituent atoms of residue 16 and residue 30, only the two α-carbon atoms (see Figure 4) were considered for further analysis.

Helical disruptions are characterized by conformational transitions from highly packed helices to irregular and flexible loops or random coils. Taking into account that higher R_g values denote significant conformational changes, which in our case means partial deletion of the helical content, we expected that also distances between the edges of the helix might present appropriate values (decreased values) that can support our hypothesis.

The random models predict an increase in distance (with 0.19 nm) between the 4P and 7P models, even though the distance between the helical edges for 9P model was larger (2.10 nm) in comparison to the other two models. In other words, for the random models where proline residues were situated all over the input m-HTT structure, it is difficult to provide a clear rule that might describe the disruption processes.

The correlation between helical disruption and C-alpha distances was analyzed for models with same number of P mutations but on different mutation points (for example: 9P(E) and 9P(EM)) and for different numbers of mutations but on the same mutation points (4P(E) and 9P(E)). When a higher number of proline residues (9P model) was placed directly on the helix, the distances between the edges decreased. The largest distance of 2.16 nm was noted for the 9P random (9PR) model, while the smallest distance of 1.66 nm was seen for the same model but with point mutations on the edges and in the middle of the helix (9P(EM)).

As expected, as the number of mutations increases, the spot of mutation becomes crucial. From the plotted results (Figure 5), we may consider that starting with a higher number of mutations (>9P), the occupied mutation spots that favor the helical disruptions are on the edges and in the middle of the helix.

Root Mean Square Fluctuations on Helical Conformation. Although the RMSF values within the random models decreased with the increased number of proline residues (0.24 nm for 4P, 0.18 nm for 7P models and 0.16 nm for 9P model), the maximum RMSF value (of 0.25 nm) was related to 9P mutation model with mutation spots at the edges and in the middle of the helix.

The increased RMSF values (Figure 6, right) suggest a partial increase in the structures' flexibility which can be assigned to partial helical disruptions. In accordance to lower R_g values at the level of the helix (for 9P(EM)), the higher RMS fluctuations (0.24 and 0.25 nm) were observed for edges and middle mutation spots for 7P and 9P models.

The largest difference between models was related to the 4P and 9P models with mutation points on the edges and on the edges and in the middle of the helix. For 4P(E), the average

https://dx.doi.org/10.1021/acschemneuro.0c00493
ACS Chem. Neurosci. 2020, 11, 2881−2889

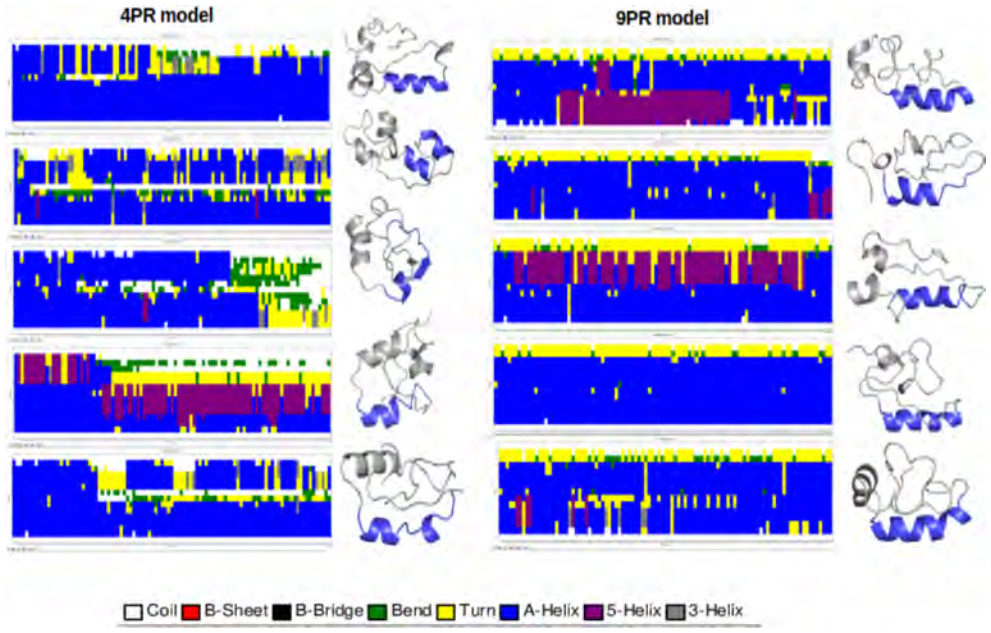

Figure 7. Secondary structure of 4P and 9P random models and the selected corresponding simulated structures (per run) on the right, with the resulting helical content (in blue). Each longitudinal plot represents one run.

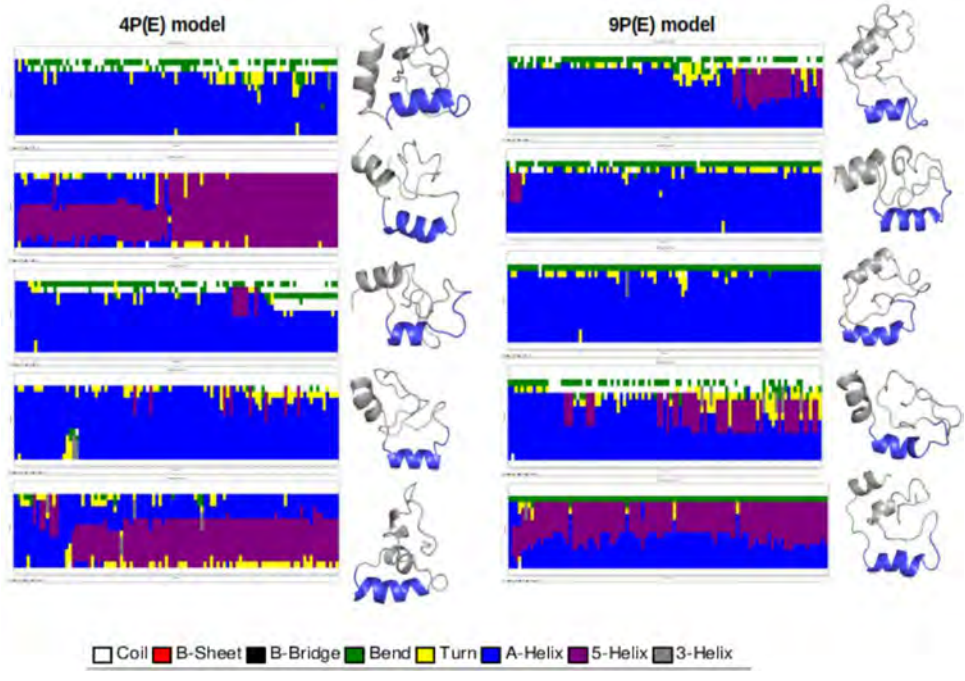

Figure 8. Secondary structure of 4P and 9P edges models and the selected corresponding simulated structures (per run) on the right, with the resulting helical content (in blue). Each longitudinal plot represents one run.

RMSF was 0.18 nm, in contrast to the RMSF value of 0.25 nm for the 9P(EM) model.

Our hypothesis is that the higher RMS fluctuations of the helix belong to transitional conformational states. The RMSF values were slightly higher for residue numbers 24−30 which leads us to a new hypothesis that the partial helical disruption occurs not only within particular number and points of mutations, but also from a certain direction. We must point out that the mutation spots and P residue numbers were situated symmetrically on both helical edges.

Secondary Structure Analysis. The secondary structure analysis was made explicitly on the helical content (A-helix, 5-helix, and 3-helix) starting from residue number 16 to residue number 30, using the DSSP[17] analysis tool incorporated in the GROMACS[18] simulation package. For random models (Figure 7), the structural elements were comparable and we observed all types of helical conformations, bends, turns, and coils. The starting configuration at the level of the helix for the random models, as for the other two sets of models, was entirely helical.

Although the mutated Q residues into P residues were all over the input sequences for random models, the presence of

https://dx.doi.org/10.1021/acschemneuro.0c00493
ACS Chem. Neurosci. 2020, 11, 2881−2889

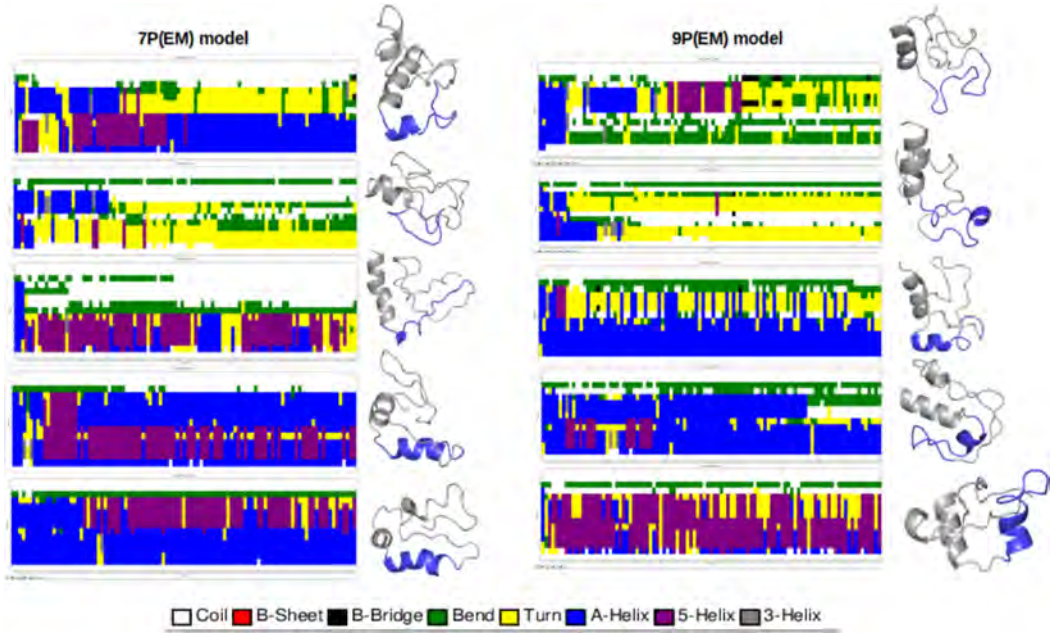

Figure 9. Secondary structure of edges-middle models and the selected corresponding simulated structures (per run) on the right, with the resulting helical content (in blue). Each longitudinal plot represents one run.

at least one P residue at the helical level favored its conformational disruption. However, this deletion presented no involvement into the significance of the mutations from a quantitative point of view. The overall structural changes between the models with lower number (4PR) and higher number (9PR) of Q mutated residues were almost the same, as shown in Figure 7.

Regarding the P residues distribution, the only difference between the edges and edges-middle models, as input structures, was one single Q residue from the middle of the helix that was mutated into P residue. In these models, the number of point mutations becomes more relevant with respect to the helical disruption.

The number of residues forming helices decreases with the increased number of P residues for the edges models (Figure 8). At this point, we can assume that once the P residues occupied a favorable mutated spot, the increased number of mutations in that particular spot promotes greater structural changes.

From the polyQ number point of view, after the 4P mutation, the entire input structure contained 41 Q residues. On the other hand, after the 9P mutation, the polyQ tract decreased to 36 Q residues which is also considered to be the Huntington disease's threshold. Moreover, the input helical content for residues 16−30, on both 9P(E) and 4P(E), was the same. As a result of these simulations, the mutated 9P(E) model presented a lower number of helical elements. On the other hand, when 9P models were compared (Figures 8 and 9) we observed that the edges-middle model presented the lowest number of resulting helical residues from all of the 9P models.

The increased values of RMS fluctuations shown in Figure 6 (right) are in agreement with the decreased number of residues that are still presenting helical content (Figures 8 and 9) by the end of the simulation. This confirms again that, for a certain number of mutations (9P mutations for example) that must act as a threshold unit, the spot of mutation (random, edges, or edges-middle) becomes crucial for the helical content's disruption that must be considered.

From all of the mutated structures, the 7P and 9P edges-middle models (Figure 9) presented the lowest number of remaining helical residues. Most of the initial helical content of the 7P(EM) and 9P(EM) models converted into bends, turns, and random coils. For the 7P edges-middle models, the presence of turn conformations is lower in comparison to the 9P(EM) model, where the turns from 7P(EM) changed into a higher number of random coils.

For the edges-middle models, the structural changes presented the lowest number of resulting helical residues from all of the input structures. In contrast, the edges models were seen to adopt more 5-helical conformations which are structural reactions to single point amino acids mutations into pre-existing α-helical content.[19] The interchanges between α-helices and 5-helices can be assigned to alterations into the protein's functionality.[20] As seen in Figure 8, the 9P(E) and 7P(E) models are the most abundant in these type of helices.

Although our interest was mainly focused on the helical content at the level of residue numbers 16−30, it is important to outline that the presence of α-helix conformations from the N-terminal HTT domain involves high overall structural stability. As we mentioned before, the number of Qs in the mutated structures was 36, 38, and 41, respectively, and it was demonstrated that the helical conformation gradually increases with the increase of polyQ tract length.[21] In our models, more α-helical configurations at the N-terminal domain were observed for mutation points distributed randomly along the helix. Additionally, higher structural stability on Htt mutants was seen to have antagonistic effects on physiological behaviors, and thus, less structural stability induced by the presence of coil, turn, and bend conformations might decrease the potential polyQ aggregation rates.

The correlation between RMSF, alpha-C distances, and DSSP analysis demonstrates that multiple GLN into PRO mutations in our models induce large structural changes with high potential impact on the HTT mutant dynamical behavior. From the well-known premise that PRO residues favor disruption of the helical content, our tested sequences promote

https://dx.doi.org/10.1021/acschemneuro.0c00493
ACS Chem. Neurosci. 2020, 11, 2881−2889

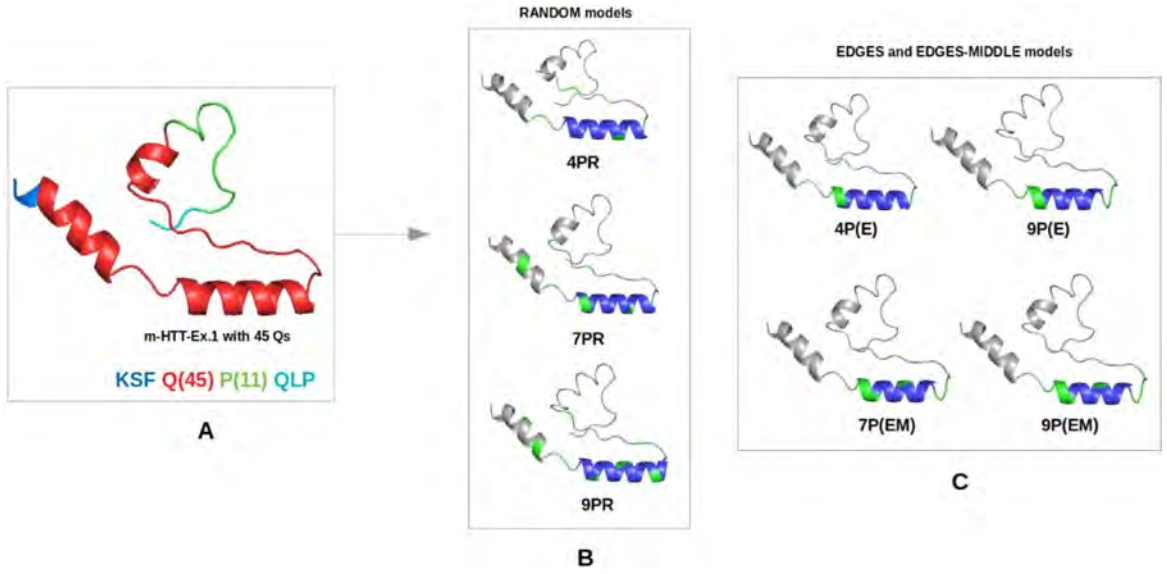

Figure 10. Input structures (B, C) modeled from m-HTT protein with 45 Qs (A), and their starting configuration points. The input m-HTT with 45 Qs was modeled in PyMol[25] and Avogadro[24] software using the PDB files encoded 4FEB,[22] 4FE8,[22] and 3IOW[23] as input crystal structures. All the mutations (colored in green) illustrated in (B) and (C) were performed in PyMol with the *mutagenesis* option, from where the right starting-ending terminals of the proline residues were selected.

the transitions from helical into loop configurations. As an ultimate effect of it, the toxic helical conformations might become less stable and highly soluble in solvents.

These results can help scientists in this field to generate (at a theoretical or experimental level), through specificity (in terms of number of mutations and spots of mutation), higher rates of helical disruption and perhaps not only in Huntington's disease but also in other amyloid-like structured diseases where identical polymerized residues can fold into distinctive amyloid configurations.

■ SCIENTIFIC CONCEPTS AND METHODS

The present study was conducted on three different types of mutations. Considering the previously reported theoretical data[10] which supports the hypothesis that cerebral inclusions are being formed for polyQ tracts longer than 36−40 Qs, the starting sequence used for molecular dynamics (MD) simulations contained the last three residues from the N-terminal domain (KSF), the 45 Qs considered as the mutation itself, the 11 proline residues (P11), and the next three residues (QLP) from the PRD. The input m-HTT with 45 Q residues was obtained from three validated and published PDB files (4FEB,[22] 4FE8,[22] and 3IOW[23]) as follows: the N-terminal section KSF (with 7 Qs) was modeled from the 4FEB file to get the required α-helical content; the helix of interest (residues 16−30) was modeled from the 4FE8 (chain C) file (the HIS residues were changed into GLN, preserving the same residue's orientation); the last 6Q 11P QLP sequence from 3IOW file was used to obtain the loop configurations at the PRD level. To obtain the full 45 Qs α-helical content, we modeled the other Qs in Avogadro24 software where we connected the Q residues according to their chirality. The full Ex.1 sequence was not used in this study because our interest was to observe dynamical and structural changes strictly on the polyQ tract (at the level of 16−30 Qs) as a result of several specific mutations.

The purpose of these mutations (Figure 10), where several Q residues were mutated into P residues, was to act as an adversary factor at the mutant level by disrupting the helical conformation and consequently, turning the entire SS into loops. Most of the proline residues in the Htt (WT or mutant) sequence tend to adopt random coil and/or loops; therefore, we considered the possibility that a specific proline sequence (in terms of number and places) might be able to break the helical conformation of the mutant.

In the first model, four Q residues were mutated into P and the mutations were made at the edges of the helical content (model 4P(E)). For the second model, the mutated seven Q residues were considered at the edges of the helix (3 P residues on each side) and one P residue right in the middle of it (7P(EM)). In the same manner, the model with nine mutation spots was divided into two distinctive structures: one with 4 P residues mutated on the edges of the helix and another P residue closer to the PRD (9P(E)), while in the other structure the proline closer to PRD was inserted this time in the middle of the (large) helix.

A control model was designed for each type of mutation where the same number of proline residues was placed randomly along the m-Htt sequence (Figure 10B). It is important to mention that also the random models (xPR) presented at least one proline residue (for 4PR) at the level of the helix. For the other two models (7PR and 9PR), the helical content consisted of two and three P residues, respectively.

All-atom simulations were performed using the latest version of the GROMACS package[18] and united-atom GROMOS43a2 force field.[26] The structures were solvated with simple point charge (SPC) water model[27] in a cubic box of 1.0 nm distance between the model of interest and the box edges. In order to neutralize the systems, counterions (chloride ions) were added. The minimization step was carried out by steepest descent method and the systems reached their minimum potential energies in less than 550 ps.

Prior multiple all-atom MD simulations for 100 ns the structures were equilibrated in two stages. The NVT ensemble (with constant number of particle, volume, and temperature) and NPT ensemble (with constant number of particle, pressure, and temperature) were performed for 10 ns, where the system temperature was kept constant at 300 K. Bonds involving hydrogen atoms were constrained using LINCS (LINear Constraint Solver) algorithm.[28] During the simulations, the temperature and pressure couplings were on and a modified Berendsen thermostat and Parrinello−Rahman barostat were used. For a higher accuracy the temperature coupling was made using two coupling groups and a time constant of 0.1 ps. The isotropic pressure coupling was set at 1 bar with a time constant of 2.0 ps.

https://dx.doi.org/10.1021/acschemneuro.0c00493
ACS Chem. Neurosci. 2020, 11, 2881−2889

CONCLUSIONS

Although the random models of 4P, 7P, and 9P mutations did not suggest specific behavioral patterns, the edges and edges-middle models presented structural and dynamical characteristics that supported our initial hypothesis.

At the m-HTT-Ex.1 compactness level, we observed that R_g values increases by increasing the number of P mutated residues. On the other hand, for helical content, the R_g results showed significant decreases in the averaged values which were afterward correlated with high RMS fluctuations (0.25 nm highest value for 9P(EM) model) and consequently to potential disruptions of the helical conformation. In addition, the edges-middle mutation spots point to greater impact on the helical disruption. The 4P(R) model presented the highest R_g value of 0.79 nm, while the lowest average value of 0.71 nm was obtained for 9P(EM).

The largest value of Cα−Cα distances (2.16 nm) observed for moderate helical disruption was noted for 9P models with point mutations situated randomly along the helix, while the smallest distance (of 1.66 nm) between the helical edges was seen for 9P model with point mutations on the edges and in the middle of the helix. These results were correlated with the secondary structure analysis. Considering the presented results, the 4P models (with 41 Q residues) outlined less structural changes with higher helical content in comparison to the other two (7P and 9P) models.

The present study is based on several mutations along the polyQ tract with certain polyP sequences, for which in gene therapy this replacement within the two residues (GLN into PRO) might reduce the formation of helical structures. Furthermore, the results showed no β-sheet formation in our trajectories, and consequently, our results are in agreement with the hypothesis that proline is able to break both α-helix and β-sheet contents. Thus, we propose a quantitative mutational threshold of 9P residues with spots of mutation on the edges and in the middle of the helix for higher rates of helical disruption. As a potential perspective of these findings, further investigations from a dynamical point of view are mandatory in order to gain insights into how exactly these type of mutants interact with other partners, other HTT mutants, or receptors.

AUTHOR INFORMATION

Corresponding Author

Vasile Chiş − *Faculty of Physics, Babeş-Bolyai University, RO-400084 Cluj-Napoca, Romania;* orcid.org/0000-0002-0935-4134

Author

Sanda Nastasia Moldovean − *Faculty of Physics, Babeş-Bolyai University, RO-400084 Cluj-Napoca, Romania*

Complete contact information is available at: https://pubs.acs.org/10.1021/acschemneuro.0c00493

Author Contributions

S.N.M. designed the analysis, collected the data, analyzed data and wrote the original draft. V.C. conceived and designed the analysis, analyzed data, and revised the manuscript.

Notes

The authors declare no competing financial interest.

ACKNOWLEDGMENTS

S.N.M. acknowledges the support of the CNCS-UEFISCDI Romania, Grant PN-III-P1-1.1-TE-2016-0628. V.C. acknowledges the support of the CNCS-UEFISCDI Romania, Grant PN-III-P4-ID-PCCF-2016-0112.

REFERENCES

(1) Roos, R. A. C. (2010) Huntington's disease: a clinical review. *Orphanet J. Rare Dis. 5*, 40.

(2) Hoffner, G., and Djian, P. (2015) Polyglutamine Aggregation in Huntington Disease: Does Structure Determine Toxicity? *Mol. Neurobiol. 52*, 1297−1314.

(3) Moldovean, S., and Chiş, V. (2020) Molecular Dynamics simulations applied to structural and dynamical transitions of the HTT protein: A review. *ACS Chem. Neurosci. 11*, 105−120.

(4) Goldschmidt, L., Teng, P. K., Riek, R., and Eisenberg, D. (2010) Identifying the amylome, proteins capable of forming amyloid-like fibrils. *Proc. Natl. Acad. Sci. U. S. A. 107*, 3487−3492.

(5) Büning, S., Sharma, A., Vachharajani, S., Newcombe, E., Ormsby, A., Gao, M., Gnutt, D., Vöpel, T., Hatters, D. M., and Ebbinghaus, S. (2017) Conformational dynamics and self-association of intrinsically disordered Huntingtin exon 1 in cells. *Phys. Chem. Chem. Phys. 19*, 10738−10747.

(6) Dobson, C. M. (2004) *Seminars in Cell and Developmental Biology* (Ellis, J., Ed.), pp 3−16, Vol. *15*, Associated Press, New York.

(7) Baias, M., Smith, P. E. S., Shen, K., Joachimiak, L. A., Żerko, S., Koźmiński, W., Frydman, J., and Frydman, L. (2017) Structure and Dynamics of the Huntingtin Exon-1 N-Terminus: A Solution NMR Perspective. *J. Am. Chem. Soc. 139*, 1168−1176.

(8) Morris, A., et al. (1992) Stereochemical quality of protein structure coordinates. *Proteins: Struct., Funct., Genet. 12*, 345−364.

(9) Williamson, M. P. (1994) The structure and function of proline-rich regions in proteins. *Biochem. J. 297*, 249−260.

(10) Kay, B. K., Williamson, M. P., and Sudol, M. (2000) The importance of being proline: the interaction of proline-rich motifs in signaling proteins with their cognate domains. *FASEB J. 14*, 231−241.

(11) Klein, F., Pastore, A., Masino, L., Zederlutz, G., Nierengarten, H., Oulad-Abdelghani, M., Altschuh, D., Mandel, J., and Trottier, Y. (2007) Pathogenic and Non-pathogenic Polyglutamine Tracts Have Similar Structural Properties: Towards a Length-dependent Toxicity Gradient. *J. Mol. Biol. 371*, 235−244.

(12) Bhattacharyya, A., Thakur, A. K., Chellgren, V. M., Thiagarajan, G., Williams, A. D., Chellgren, B. W., Creamer, T. P., and Wetzel, R. (2006) Oligoproline effects on polyglutamine conformation and aggregation. *J. Mol. Biol. 355*, 524−535.

(13) Atwal, R. S., Xia, J., Pinchev, D., Taylor, J., Epand, R. M., and Truant, R. (2007) Huntingtin has a membrane association signal that can modulate huntingtin aggregation, nuclear entry and toxicity. *Hum. Mol. Genet. 16*, 2600−2615.

(14) Lakhani, V. V., Ding, F., and Dokholyan, N. V. (2010) Polyglutamine Induced Misfolding of Huntingtin Exon1 is Modulated by the Flanking Sequences. *PLoS Comput. Biol. 6*, No. e1000772.

(15) Kar, K., Jayaraman, M., Sahoo, B., Kodali, R., and Wetzel, R. (2011) Critical nucleus size for disease-related polyglutamine aggregation is repeat-length dependent. *Nat. Struct. Mol. Biol. 18*, 328.

(16) Priya, B. S., and Gromiha, M. M. (2019) Structural insights into the aggregation mechanism of huntingtin exon 1 protein fragment with different polyQ lengths. *J. Cell. Biochem. 120*, 10519−10529.

(17) Kabsch, W., and Sander, C. (1983) Dictionary of protein secondary structure: Pattern recognition of hydrogen-bonded and geometrical features. *Biopolymers 22*, 2577−2637.

(18) Van Der Spoel, D., Lindahl, E., Hess, B., Groenhof, G., Mark, A. E., and Berendsen, H. J. (2005) GROMACS: fast, flexible, and free. *J. Comput. Chem. 26*, 1701−1718.

(19) Cooley, R. B., Arp, D. J., and Karplus, P. A. (2010) Evolutionary origin of a secondary structure: π-helices as cryptic but widespread insertional variations of α-helices enhancing protein functionality. *J. Mol. Biol. 404*, 232−246.

(20) Keefe, L. J., Sondek, J., Shortle, D., and Lattman, E. E. (1993) The alpha aneurism: a structural motif revealed in an insertion mutant of staphylococcal nuclease. *Proc. Natl. Acad. Sci. U. S. A. 90*, 3275−3279.
(21) Nagai, Y., Inui, T., Popiel, H. A., Fujikake, N., Hasegawa, K., Urade, Y., Goto, Y., Naiki, H., and Toda, T. (2007) A toxic monomeric conformer of the polyglutamine protein. *Nat. Struct. Mol. Biol. 14*, 332−340.
(22) Kim, M. (2013) Beta conformation of polyglutamine track revealed by a crystal structure of Huntingtin N-terminal region with insertion of three histidine residues. *Prion 7*, 221−228.
(23) Kim, M., Chelliah, Y., Kim, S., Otwinowski, Z., and Bezprozvanny, I. (2009) Secondary structure of Huntington amino-terminal region. *Structure 17*, 1205−1212.
(24) Hanwell, M. D., Curtis, D. E., Lonie, D. C., Vandermeersch, T., Zurek, E., and Hutchison, G. R. (2012) Avogadro: An advanced semantic chemical editor, visualization, and analysis platform. *J. Cheminf. 4*, 17.
(25) DeLano, W. L. (2002) Pymol: An open-source molecular graphics tool. *CCP4 Newsletter On Protein Crystallography* (Ballard, C., and Howard-Eales, M.), pp 82−92, Vol. *40*.
(26) Van Gunsteren, W. F., Billeter, S. R., Eking, A. A., Hiinenberger, P. H., Kriiger, P., Mark, A. E., Scott, W. R. P., and Tironi, I. G. (1996) *Biomolecular Simulation, The GROMOS96 Manual and User Guide. Vdf Hochschulverlag AG an der ETH Zürich*, pp 1−1042, Zürich, Switzerland.
(27) Berendsen, H. J. C., Postma, J. P. M., Van Gunsteren, W. F., and Hermans, J. (1981) Intermolecular Forces, Interaction models for water in relation to protein hydration. In *Intermolecular Forces* (Pullman, B., Ed.), pp 331−342, D. Reidel Publishing Company, Dordrecht.
(28) Hess, B., Bekker, H., Berendsen, H. J. C., and Fraaije, J. G. E. M. (1997) LINCS: A Linear Constraint Solver for Molecular Simulations. *J. Comput. Chem. 18*, 1463−1472.

https://dx.doi.org/10.1021/acschemneuro.0c00493
ACS Chem. Neurosci. 2020, 11, 2881−2889